Molecular Structure and Phase Diagram of the Binary Mixture of *n*-Heptane and Supercritical Ethane: A Gibbs Ensemble Monte Carlo Study

Marcus G. Martin,† Bin Chen, and J. Ilja Siepmann*

Departments of Chemistry and of Chemical Engineering and Materials Science, University of Minnesota, 207 Pleasant St. SE, Minneapolis, Minnesota 55455-0431

Received: September 10, 1999; In Final Form: December 13, 1999

Pressure-composition and temperature-composition phase diagrams are computed for the binary mixture of *n*-heptane and supercritical ethane using four different molecular models of increasing complexity. The ethane and heptane molecules were described using either (i) single-site Lennard−Jonesium (LJ) with fixed well-depth and size parameters, (ii) single-site LJ with temperature-dependent well depths, (iii) chains of methyl and methylene pseudo-atoms interacting via LJ potentials placed at the positions of all carbon nuclei, or (iv) an explicit-hydrogen representation with LJ interaction sites placed both at the carbon nuclei and at the centers of all carbon−hydrogen bonds. For comparison, simulations were also performed for the binary mixture of *n*-heptane and helium using the pseudo-atom model for the *n*-heptane molecules. All four models produce phase diagrams for the ethane/*n*-heptane mixture that are in reasonable agreement with experiment. However, the accuracy of the calculated phase diagrams improves markedly with increasing complexity of the model (and therefore increasing computational requirements). In both the liquid (*n*-heptane-rich, higher specific density) and supercritical (ethane-rich, lower specific density) phases center-of-mass radial distribution functions appear to show more enhanced structures for the two single-site models than the united-atom and explicit-hydrogen force fields. However, the number integrals of these radial distribution functions are strikingly similar for all models, that is the differences in molecular shape do not lead to a difference in the clustering of the solvent molecules around the solute. In particular, preferential solvation of *n*-heptane by ethane is not observed in the supercritical phase. Analysis of the contributions of the liquid and the supercritical phases to the decrease of the Gibbs free energy of transfer of *n*-heptane with increasing pressure suggest that the enhanced solubility of *n*-heptane in high-pressure supercritical ethane can be attributed to two causes of roughly equal importance: "Pulling" of *n*-heptane into the supercritical phase by an increased density of ethane that acts as a nonspecific solvent, and "pushing" *n*-heptane out of the liquid phase by an increased concentration of ethane.

1. Introduction

The critical point marks the high-temperature end of the vapor−liquid coexistence line in a pressure−temperature phase diagram and the supercritical fluid (SCF) region is defined as the part of the phase diagram characterized by temperatures and pressures higher than the critical temperature and pressure, respectively. More than 100 years ago, Hanny and Hogarth discovered the ability of SCFs to act as powerful solvents.[1] However, SCF extraction did not become an industrially viable process until the late 1970s.[2−4] The most famous example of a SCF extraction is the decaffeination of green coffee beans with supercritical CO_2 as the solvent.[5] Currently, SCFs are also used in the removal of nicotine from tobacco, the extraction of hops, flavors, spices, and perfumes from natural products, the extraction of lower boiling products from the residues of crude oil distillation, and the separation of solvents and monomers from polymers.[2−4] Separations of multicomponent mixtures with SCF solvents use differences in volatility (the driving force in ordinary distillations) and differences in the specific solute−solvent interactions (the driving force in ordinary liquid extraction).

Despite the great promise for SCF technology, a fundamental understanding of SCFs is still lacking. Of great interest is whether the distribution of supercritical solvents is relatively homogeneous on the microscopic scale, or whether there is a pronounced clustering of solvent molecules around solutes.[6−18] Measurements of the partial molar volume of the solute give information on the long-range condensation of supercritical solvents around the solutes,[6−8] whereas spectroscopic techniques are used to study the local ordering around a specific spectroscopic probe.[9−14] Solvent clustering has also been investigated using integral equation and mean-field theories[15−17] and molecular simulations.[15,18] The issue of nonrandom mixing is of particular importance for the equation-of-state−based modeling of supercritical phase equilibria.[18−20]

The applicability of an SCF extraction can be determined from knowledge of the phase diagram which provides, among other things, information on (i) the capacity of the SCF solvent, (ii) the amount of SCF solvent that dissolves in the liquid phase, (iii) the selectivity of the SCF solvent to separate different solutes, (iv) the dependence of SCF solvent properties on temperature and pressure, and (v) the extent of the two-phase area that limits the external conditions available for extractions.

Computer simulation is an ideal tool to investigate SCF systems in microscopic detail[15,18,21−29] and to make quantitative

† Present address: Computational Biology and Materials Technology, Sandia National Laboratories, PO Box 5800, Albuquerque, NM 87185-1111.

* Corresponding author: siepmann@chem.umn.edu.

10.1021/jp993212v CCC: $19.00 © 2000 American Chemical Society
Published on Web 02/17/2000

TABLE 1: Lennard−Jones Parameters for the CC, ST, TraPPE-UA, and TraPPE-EH Force Fields

force field	interaction site	ϵ/k_B (K)	σ (Å)
CC	ethane	236	4.25
CC	*n*-heptane	418	6.08
ST 336 K	ethane	234.30	4.2338
ST 336 K	*n*-heptane	484.76	6.0471
ST 450 K	ethane	228.15	4.2338
ST 450 K	*n*-heptane	456.82	6.0471
TraPPE-UA	CH_3	98	3.75
TraPPE-UA	CH_2	46	3.95
TraPPE-UA	He	4	3.11
TraPPE-EH	(C)−H_3	4.0	3.30
TraPPE-EH	(C)−H_2	5.0	3.65
TraPPE-EH	C(−)H	15.3	3.31

predictions of phase equilibria.[30−32] In this article we present a detailed investigation for the binary ethane/*n*-heptane mixture using four different models: single-site Lennard−Jonesium with parameters determined by the critical constants (CC), single-site Lennard−Jonesium with temperature-dependent energy parameters as suggested by Sun and Teja (ST),[33] the Transferable Potentials for Phase Equilibria United-Atom description (TraPPE-UA),[34] and the TraPPE Explicit-Hydrogen model (TraPPE-EH).[35] From comparison of these different models, we can learn what type of model is required to describe both the phase equilibria and the microscopic structure of the SCF mixtures. From comparison with simulations for helium/*n*-heptane mixtures, we can learn about the differences between a "good" (e.g. ethane) and a "bad" (e.g. helium) supercritical solvent for *n*-heptane.

The remainder of this article is organized as follows. First, the details of the four molecular models are described, followed by a description of the simulation details. Thereafter, we report the results of our calculations (phase diagrams and microscopic structures) and discuss their implications for the supercritical solvation mechanism.

2. Molecular Models

All four models considered here describe the nonbonded interactions solely by pairwise-additive Lennard−Jones (LJ) 12−6 potentials

$$u(r_{ij}) = 4\epsilon_{ij}\left[\left(\frac{\sigma_{ij}}{r_{ij}}\right)^{12} - \left(\frac{\sigma_{ij}}{r_{ij}}\right)^{6}\right] \quad (1)$$

where r_{ij}, ϵ_{ij} and σ_{ij} are the separation, LJ well depth, and LJ size, respectively, for the pair of interaction sites i and j. A spherical potential truncation at 14 Å (CC, ST, TraPPE-UA) or 9 Å (TraPPE-EH) was used for all bead−bead interactions, and analytical tail corrections (for internal energies, pressures, and chemical potentials) were added for distances beyond the cutoff.[36] The force fields specify the parameters for interactions between like atoms, and these parameters are used to compute the interactions between unlike atoms according to the standard Lorentz−Berthelot combining rules.[37]

The Lennard−Jones parameters used for all four models are listed in Table 1. The first model (CC) represents each molecule as a single site with well-depth and size parameters fitted to the experimental critical temperatures and densities of ethane and *n*-heptane. The second model, proposed by Sun and Teja (ST),[33] also treats each molecule as a single site, but it has an ϵ parameter that is a function of temperature. The ST model was fitted to experimental vapor pressures of the *n*-alkanes. The temperature dependence of the ϵ parameter of a given molecule allows one to adjust the temperature dependence of the heat of vaporization for that molecule, thereby to capture the differences in acentric factors for the *n*-alkanes, which can be attributed to their different shapes and the effect of changing conformation with changes in temperature for the longer alkanes.

TABLE 2: Bonded Parameters for the TraPPE-UA and TraPPE-EH Force Fields

stretch	r_0 (Å)			
CH_x−CHy	1.54 (fixed)			
bend	θ_0	k_θ/k_B (K)		
CH_x−(CH_2)−CH_y	114	62 500		
torsion	c_0/k_B (K)	c_1/k_B (K)	c_2/k_B (K)	c_3/k_B (K)
CH_x−(CH_2)−(CH_2)−CH_y	0	335.03	−68.19	791.32

The third model is the united-atom version of the transferable potentials for phase equilibria (TraPPE-UA) force field,[34,38] which combines hydrogens and the carbon they are bonded to into a single interaction site centered at the carbon position. Intramolecular interactions for the TraPPE-UA model consist of fixed bond lengths, a harmonic bond bending potential,[39] a cosine series dihedral angle potential,[40] and Lennard−Jones interactions for pseudo-atoms separated by more than three bonds. The TraPPE-UA model was fitted to the liquid coexistence densities and critical temperatures of the alkanes.

The fourth model is the TraPPE-EH model,[35] which uses Lennard−Jones interaction sites positioned at the carbon atoms and at the midpoint of the carbon−hydrogen bonds. A similar set of bonded interaction potentials as in the TraPPE-UA model is used (see Table 2). The TraPPE-EH model was fitted to reproduce the experimental vapor and liquid coexistence densities and the critical temperature of the alkanes.

The different complexity of the four models results in rather different computational requirements. Although the amount of CPU time required for simulations of the single-site models (CC and ST) is the same, the united-atom description (TraPPE-UA, two and seven interaction sites for ethane and *n*-heptane, respectively) results in an increase of the CPU requirements by about 1 order of magnitude, and one additional order of magnitude is needed for the change to an explicit-hydrogen description (TraPPE-EH, 8 and 23 interaction sites for ethane and *n*-heptane, respectively).

3. Simulation Details

A combination[41,42] of the Gibbs ensemble Monte Carlo (GEMC) technique[43−45] and the configurational-bias Monte Carlo (CBMC) method[46−49] was used to determine pressure-composition and temperature-composition diagrams for the binary ethane/*n*-heptane mixtures.

The isobaric−isothermal Gibbs ensemble simulations for models CC, ST, and TraPPE-UA were performed for system sizes of 800 molecules with the total volume of the two simulation boxes, and the overall mole fraction of *n*-heptane, adjusted so that both phases contained approximately 400 molecules. The TraPPE-EH simulations were performed for a system size of 400 molecules, again with a roughly equal distribution of the molecules over the two phases. Moves were selected at random with a fixed probability where the fraction of CBMC particle moves for both molecule types were adjusted manually to obtain roughly one accepted molecule swap per 10 Monte Carlo cycles, the fraction of volume moves was 0.001, and the remainder of the moves were divided according

$$P^{T}_{eth}/N_{eth} = P^{T}_{hep}/N_{hep} = P^{R}_{eth}/N_{eth} = P^{R}_{hep}/N_{hep}[=P^{CB}_{hep}/N_{hep}] \quad (2)$$

to where N_x is the total number of molecules of type x in the simulation, P_x^m is the probability of performing move type m on molecule type x, and m can be one of the following move

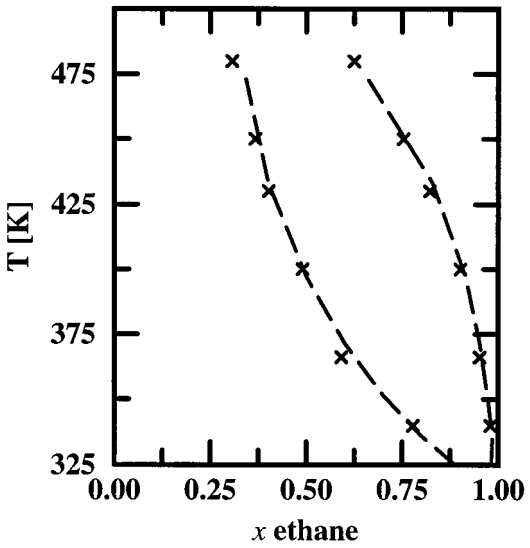

Figure 1. Temperature-composition phase diagram for the ethane/*n*-heptane mixture at a pressure of 5.5 MPa. The experimental data[53,54] are shown as dashed lines. The simulation results for the TraPPE-UA model are shown as crosses.

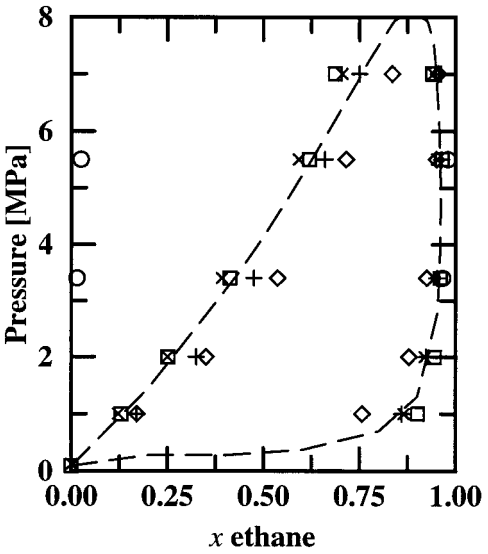

Figure 2. Pressure-composition diagram for the ethane/*n*-heptane mixture at a temperature of 366 K. The experimental data[53,54] are shown as dashed lines. The simulation results are shown for the CC (diamonds), ST (pluses), TraPPE-UA (crosses), and TraPPE-EH (squares) models. The results for simulations of the helium/*n*-heptane mixture using the TraPPE-UA model are shown as circles.

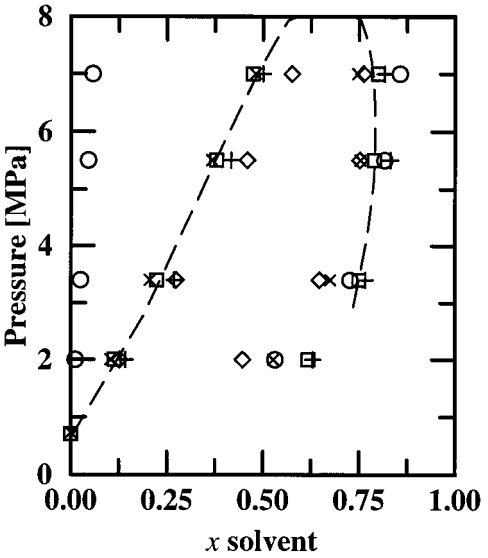

Figure 3. Pressure-composition diagram for the ethane/*n*-heptane mixture at a temperature of 450 K. Line styles and symbols as in Figure 2.

types: translation (T) of the center of mass, rotation (R) about the center of mass, and configurational-bias (CB) regrowths of part of the molecule. The latter type of move is, of course, not used for simulations of the single-site models. The maximum translational, rotational, and volume displacements were adjusted automatically to yield 50% acceptance rates for each type of molecule in each simulation box. Computational efficiency was improved by using a biased insertion with 10 trial sites for the first interaction site in a CBMC particle swap,[50,51] an additional center-of-mass−based cutoff which avoids computing unnecessary distances,[34] and a shorter potential truncation ($r_{CBMC} = 5$ Å) for use during split-energy CBMC moves, which is then corrected to the full potential ($r_{cut} = 14$ or 9 Å) with tail corrections in the acceptance rule.[52] Simulations were equilibrated for at least 100 000 MC cycles during which the chemical potentials, the pressure, and the differences in the number of molecule exchanges was monitored. The production periods consisted of 100,000 MC cycles. Standard deviations of the ensemble averages were computed by breaking the production runs into five blocks.

4. Results and Discussion

A. Temperature-Composition Diagram. Calculations of the temperature−composition diagram for the mixture of ethane and *n*-heptane were performed only for the TraPPE-UA force field at a pressure of 5.5 MPa (see Figure 1). The agreement with experiment is good across the full range of temperatures at this pressure. This demonstrates that a force field that has been fitted to subcritical vapor−liquid coexistence curves is transferable to the supercritical region.

B. Pressure-Composition Diagrams. Figures 2 and 3 show the pressure- composition diagrams for ethane/*n*-heptane mixtures at temperatures of 366 and 450 K obtained for the CC, ST, TraPPE-UA, and TraPPE-EH models. Although all four models capture the qualitative features of the 366 K phase diagram, only the TraPPE-UA and TraPPE-EH models produce quantitative agreement (except at 7 MPa). The 450 K pressure-composition phase diagram presents a more stringent test of these models, because only the TraPPE-EH force field is able to accurately predict both the composition of the liquid and supercritical phases. The TraPPE-UA model yields good results for the liquid phase, but deviates significantly for the supercritical phase, whereas CC and ST are rather inaccurate for both phases. Results for the mixture of supercritical helium and *n*-heptane using the TraPPE-UA force field are also shown, and although the composition of the supercritical phase is similar to those in the ethane/*n*-heptane simulations, the helium concentrations in the liquid phase are much lower than the corresponding results for ethane.

One of the interesting features of a supercritical fluid is that solute partitioning (and correspondingly the Gibbs free energy of transfer) changes markedly with pressure. Figure 4 reveals that all four models for the ethane−heptane mixture show similar trends of decreasing (in magnitude) Gibbs free energies of transfer for *n*-heptane between the two phases as the pressure is increased. In contrast, ΔG^* is rather independent of pressure for the helium−heptane system and remains close to the pure *n*-heptane value. It appears that the microscopic details of the

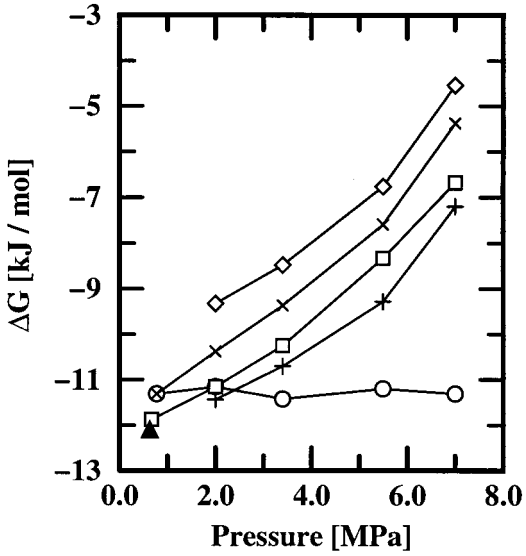

Figure 4. Gibbs free energy of transfer for *n*-heptane at a temperature of 450 K. The experimental data point[55] for pure *n*-heptane is shown as a filled triangle. The simulation results for the ethane/*n*-heptane mixture are shown for the CC (diamonds), ST (pluses), TraPPE-UA (crosses), and TraPPE-EH (squares) and are connected by lines as a guide to the eye. Simulation results for the helium/*n*-heptane are shown for the TraPPE-UA force field (open circles).

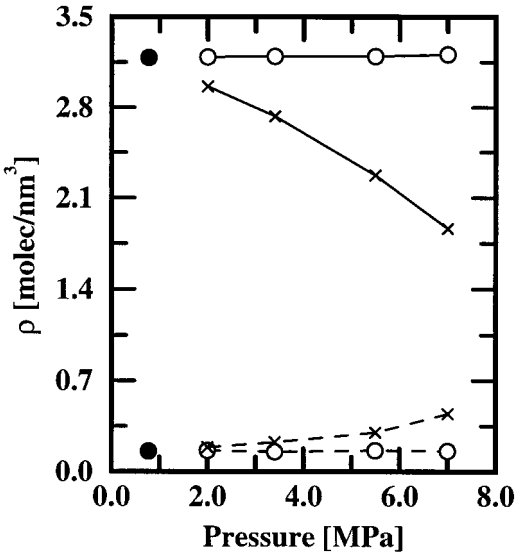

Figure 5. Number densities of *n*-heptane in mixtures with either ethane or helium at 450 K for the TraPPE-UA force field. The coexistence liquid and vapor densities of pure *n*-heptane at 450 K are shown as filled circles. The density of *n*-heptane is shown for the ethane/heptane mixture as crosses connected by a solid line (high-density phase) or by a dashed line (low-density phase). The *n*-heptane density is shown for the helium/heptane mixture as open circles connected by a solid line (high-density phase) or by a dashed line (low-density phase).

model do not have a significant effect on this trend for the ethane/*n*-heptane mixture, although the quantitative accuracy of ΔG^* does depend on the specific model. Because the CC and ST force fields yield the Gibbs free energies of transfer that are the least similar, it is clear that the specific force field parameters, and not the complexity of the force field, is the most important determinant of ΔG^* for this system. The left-most points (lowest pressures) are results obtained for pure *n*-heptane at its vapor pressure using the TraPPE-UA and TraPPE-EH models. As pointed out before, the TraPPE-EH model yields slightly better agreement with experimental vapor−liquid coexistence curves of the pure *n*-alkanes than the TraPPE-UA model.[35]

By definition, a change in the partition constant (or ΔG^*) with a change in pressure implies that the equilibrium number density in at least one of the phases must also be a function of pressure. Figure 5 shows that increasing the external pressure from 2 to 7 MPa (at $T = 450$ K) causes the *n*-heptane number density to decrease by a factor of 1.6 in the liquid phase and to increase by a factor of 2.4 in the supercritical phase. In contrast, there is essentially no change in the *n*-heptane density in either phase when ethane is replaced with helium. Thus, it is clear that a "good" supercritical solvent can affect both the liquid and supercritical phases in roughly equal measure.

To understand the role ethane plays in both phases, we compare a system of pure ethane with the behavior observed in its mixture with *n*-heptane. As one would expect for a supercritical fluid, Figure 6 shows that a system of pure ethane at 450 K has a nonlinear increase in density with pressure and yields densities higher than those of an ideal gas under the same conditions. At the lower pressures, the supercritical phase of the ethane/*n*-heptane mixture yields ethane densities that are lower than for pure ethane at the same pressure, and this is easily explained by considering the mole fraction of ethane which is significantly less than unity and *n*-heptane which also contributes to the pressure of the mixture. However, at 7 MPa the ethane density in the mixture is now actually slightly higher than that of a system of pure ethane. Thus the presence of a significant solute concentration results in an increase of the concentration

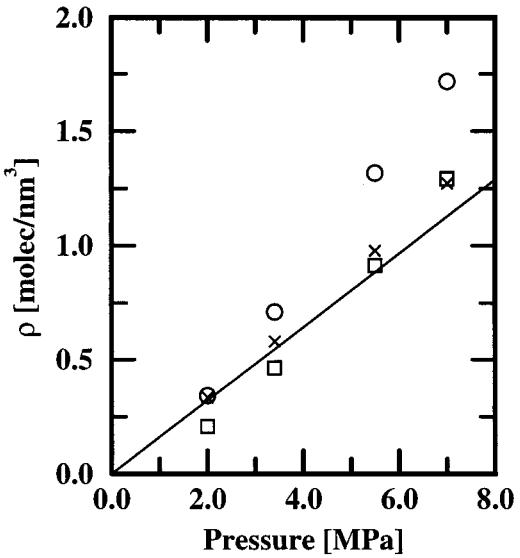

Figure 6. Densities of ethane in a mixture with *n*-heptane at 450 K for the TraPPE-UA force field. Simulation results are shown for pure ethane (crosses) and for ethane in the liquid phase (open circles) and in the supercritical phase (open squares) of the ethane/heptane mixture. The density of an ideal gas is shown as a solid line for reference.

of the supercritical solvent. For comparison, the number densities of the vapor and liquid phases of pure ethane at its normal boiling point are 0.041 and 10.9 molecules/nm^3 (experimental data[55]) and 0.040 and 10.8 molecules/nm^3 (simulation data for TraPPE-EH model). The number density of ethane in the liquid phase is always higher than found in the supercritical phase, which supports the view that the presence of ethane (the supercritical solvent) also acts on the liquid phase.

In contrast, Figure 7 shows that pure helium and the supercritical phase of the helium/*n*-heptane mixture behave essentially like an ideal gas or ideal gas mixture (although the excluded volume yields densities lower than ideality at high pressures). The density in the supercritical phase of the mixture

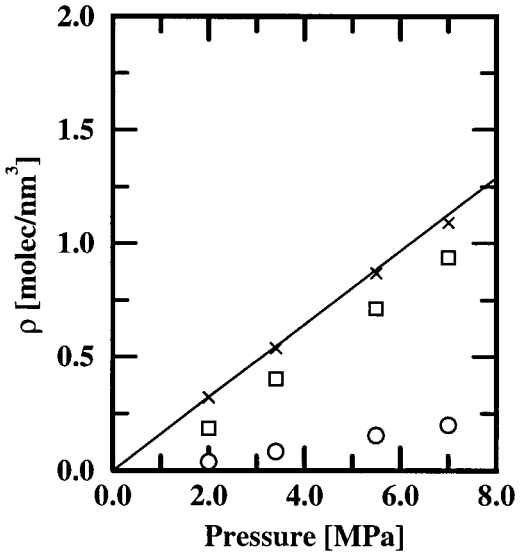

Figure 7. Densities of helium in a mixture with *n*-heptane at 450 K for the TraPPE-UA force field. Simulation results are shown for pure helium (crosses) and for helium in the liquid phase (open circles) and in the supercritical phase (open squares) of the helium/heptane mixture. The density of an ideal gas is shown as a solid line for reference.

is well rationalized by assuming that *n*-heptane contributes a partial pressure equal to the vapor pressure of pure *n*-heptane at 450 K, and that the remainder of the partial pressure arises from an ideal gas of helium. The helium density in the liquid phase is a linear function of pressure, and thus behaves as an ideal solution of a volatile compound dissolved in a liquid.

C. Microscopic Structures. Center-of-mass radial distribution functions (RDFs) calculated for the liquid and supercritical phases of the ethane/*n*-heptane mixture (CC, ST, TraPPE-UA, and TraPPE-EH models) and the helium/*n*-heptane mixture (only TraPPE-UA model) at a temperature of 450 K and a pressure of 7 MPa are shown in Figures 8 and 9. The most noteworthy feature is the dissimilarity of the RDFs obtained for the single-site (CC and ST) and articulated-chain (TraPPE-UA and TraPPE-EH) models. In contrast, there is very good agreement among the two single-site models and among the two articulated-chain models. In both the liquid and supercritical phases, the RDFs for the two single-site models show strong peaks for ethane−ethane, ethane−heptane, and heptane−heptane pairs, a behavior typical for binary Lennard−Jonesium systems. The heptane−heptane peak is strongest as should be expected from their stronger interactions (larger LJ well depth). For these models, the positions and heights of the peak in the ethane−heptane RDFs appears midway between those for ethane−ethane and heptane−heptane. Such a relatively strong peak for the unlike ethane−heptane pair is an indication for clustering of (ethane) solvent molecules around (*n*-heptane) solute molecules in supercritical phases. In contrast, the heights of the ethane−heptane peaks for the articulated-chain models (TraPPE-UA and TraPPE-EH) in the supercritical phase are significantly below those for the like pairs, a clear sign that solubilization in the supercritical phase does not rely on solvent clustering around the solute. Whereas the position, heights, and widths for the ethane−ethane peaks are similar for the single-site and articulated-chain models, the heptane−heptane peaks are much lower and much broader for the articulated-chain models, which is a reflection of the nonspherical shape of the heptane molecules. The relatively strong ethane−ethane peak observed in the liquid phases for the articulated-chain models is an indication of ethane

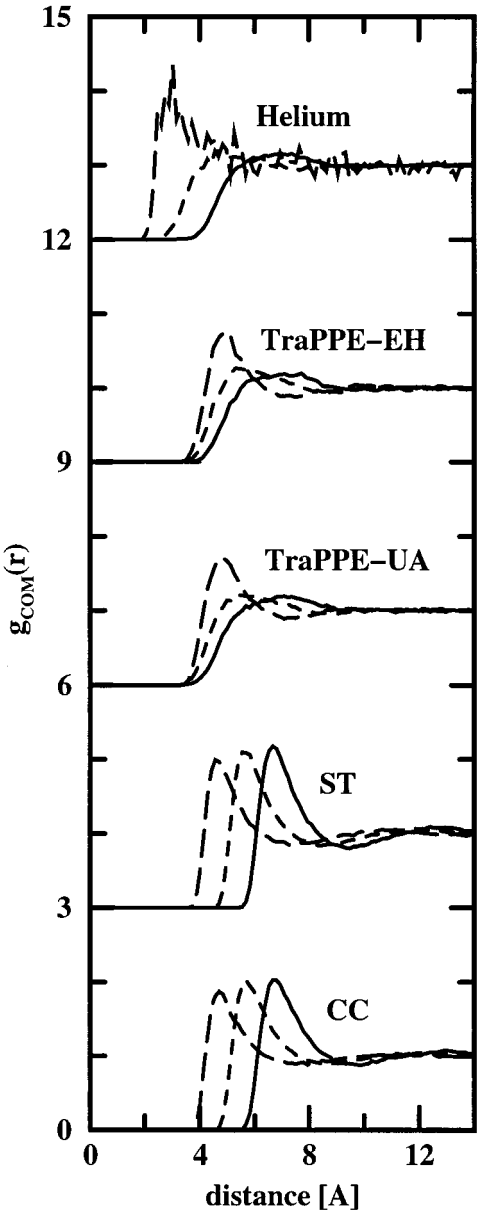

Figure 8. Center-of-mass radial distribution functions for the liquid phase of the ethane/heptane (or helium/heptane) mixture at $T = 450$ K and a pressure of 7 MPa. Radial distribution functions are shown for heptane−heptane (solid lines), ethane-heptane (short-dashed lines), and ethane−ethane (long-dashed lines). The results for the different models/mixtures are vertically displaced for clarity.

(solute) clustering in the liquid phase, which we attribute to the packing of *n*-heptane that leaves voids which can be filled by more than one ethane molecule. However, the corresponding number integrals (see below) show that on average each ethane molecule is surrounded by less than two other ethane molecules in the liquid phase.

For comparison, the RDFs for the helium/*n*-heptane mixture are also shown in Figures 8 and 9. Again, the most pronounced feature for the liquid phase is the helium−helium peak. Obviously, the helium solutes have a tendency to aggregate (but the average number of helium−helium contacts within 6 Å is less than 0.1). In contrast, the helium−helium and helium−heptane RDFs in the supercritical phase are essentially flat, as should be expected from a solvent whose properties are dominated by its repulsive core.

Figures 10 and 11 depict the number integrals (NIs) corresponding to the RDFs shown in Figures 8 and 9. For the ethane/

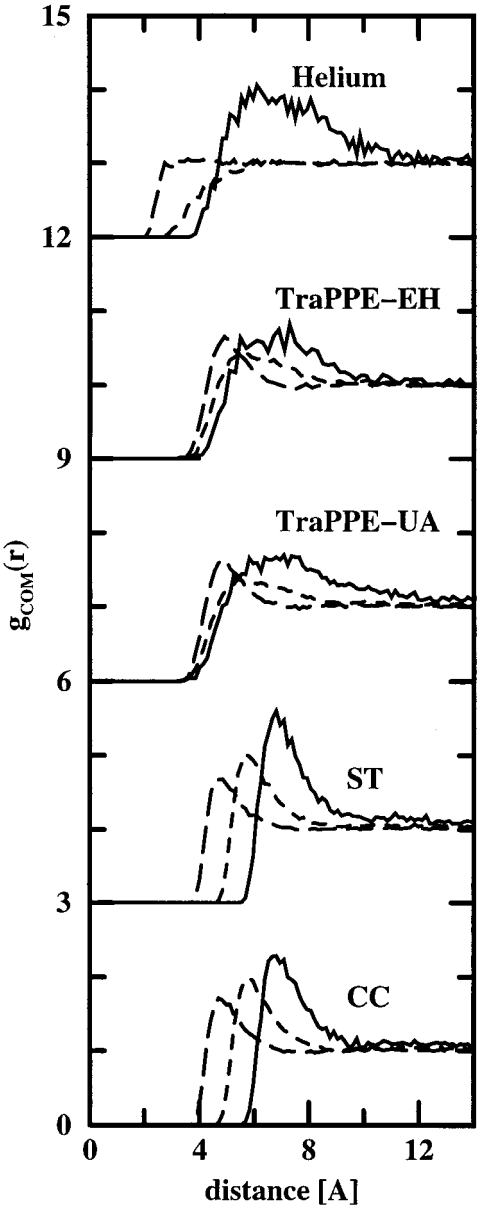

Figure 9. Center-of-mass radial distribution functions for the supercritical phase of the ethane/heptane (or helium/heptane) mixture at $T = 450$ K and a pressure of 7 MPa. Line styles as in Figure 8.

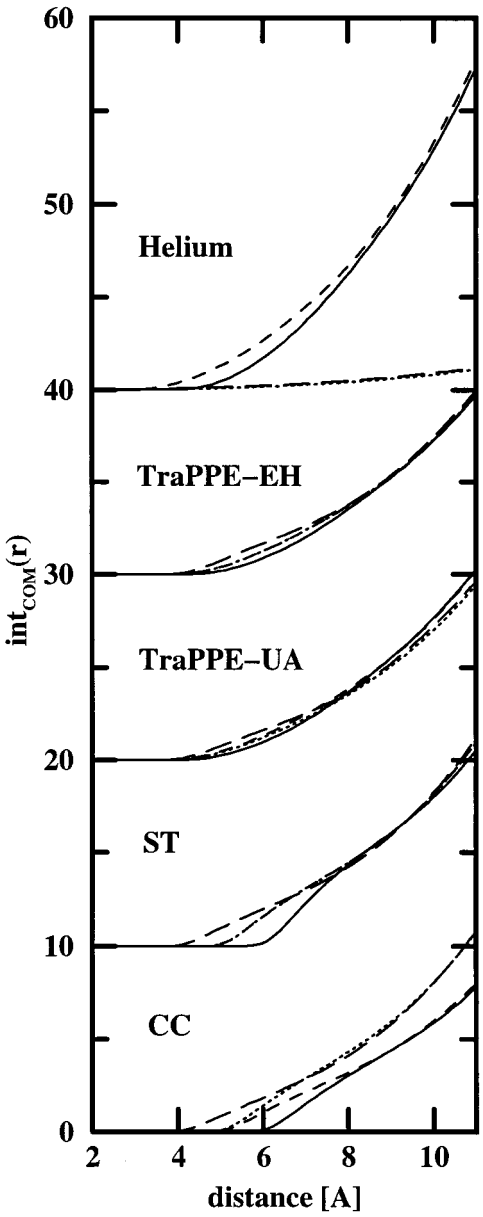

Figure 10. Number integrals of the center-of-mass radial distribution functions for the liquid phase of ethane/heptane (or helium/heptane) mixture at $T = 450$ K and a pressure of 7 MPa. Number integrals are shown for heptane surrounding heptane (solid lines), heptane surrounding ethane (short-dashed line), ethane surrounding heptane (dotted lines), and ethane surrounding ethane (long-dashed lines). The results for the different models/mixtures are vertically displaced for clarity.

heptane mixture the NIs of the single-site and articulated-chain models agree quite well, in contrast to the marked differences observed in the RDFs. Of course, this is connected to the fact that all four models yield rather similar compositions and densities for both the liquid and supercritical phases. Focusing on the supercritical phases, the most important observation is that the numbers of ethane molecules surrounding a given heptane or a given ethane molecule are very similar (and the same is also true for the numbers of heptane molecules surrounding a given heptane or a given ethane molecule). Thus, no significant preference exists for solubilization of the solute (heptane) by the solvent (ethane), and the supercritical (and liquid) phase of this system can be well described assuming random mixing of the two components. At these physical conditions, the average number of ethane molecules in the first solvation shell of heptane (within approximately 8 Å) is close to five for the supercritical phase, i.e. roughly half of what is found for a pure ethane liquid at its boiling point. The four liquid-phase NIs for the ethane/heptane mixture approach a similar value because of the roughly equimolar composition at these physical conditions. The NIs for the helium/heptane mixture differ significantly from those obtained for the ethane/heptane mixtures, mainly because of the very different compositions. It is noteworthy that even for the helium/heptane system there is little evidence for nonrandom mixing despite the much stronger heptane−heptane interactions.

The features discussed above are also observed in the RDFs and their NIs obtained at 366 K and for different pressures (see Tables 3 to 6 of the Supplementary Information).

Carbon−carbon RDFs calculated for the liquid and supercritical phases of the ethane/*n*-heptane mixture using the two articulated chain models (TraPPE-UA and TraPPE-EH) at a temperature of 450 K and a pressure of 7 MPa are shown in Figures 12 and 13. In contrast to the significant structural changes in center-of-mass RDFs observed for the change from

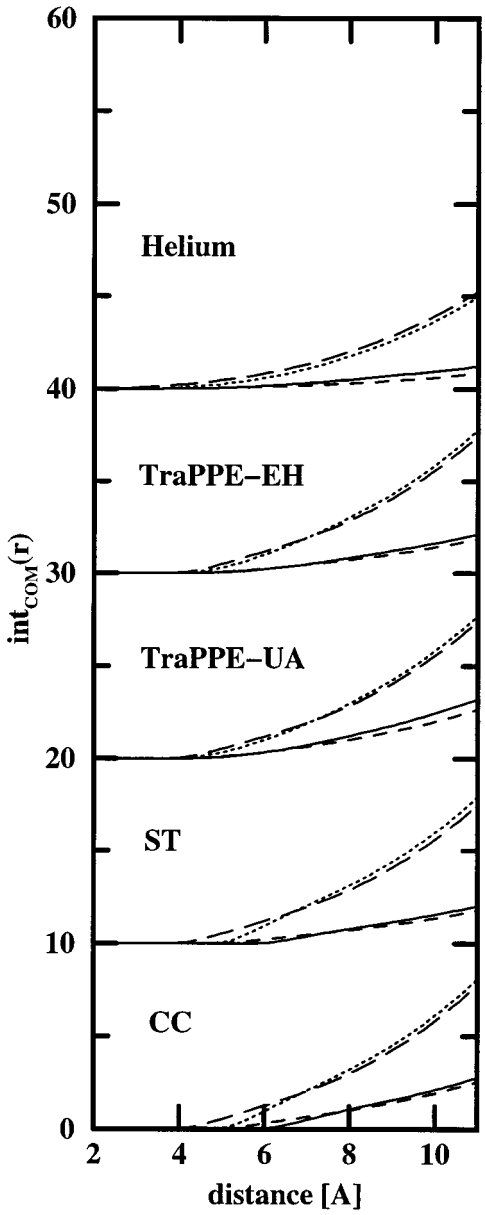

Figure 11. Number integrals of the center-of-mass radial distribution functions for the supercritical phase of ethane/heptane (or helium/heptane) mixture at $T = 450$ K and a pressure of 7 MPa. Line styles as in Figure 10.

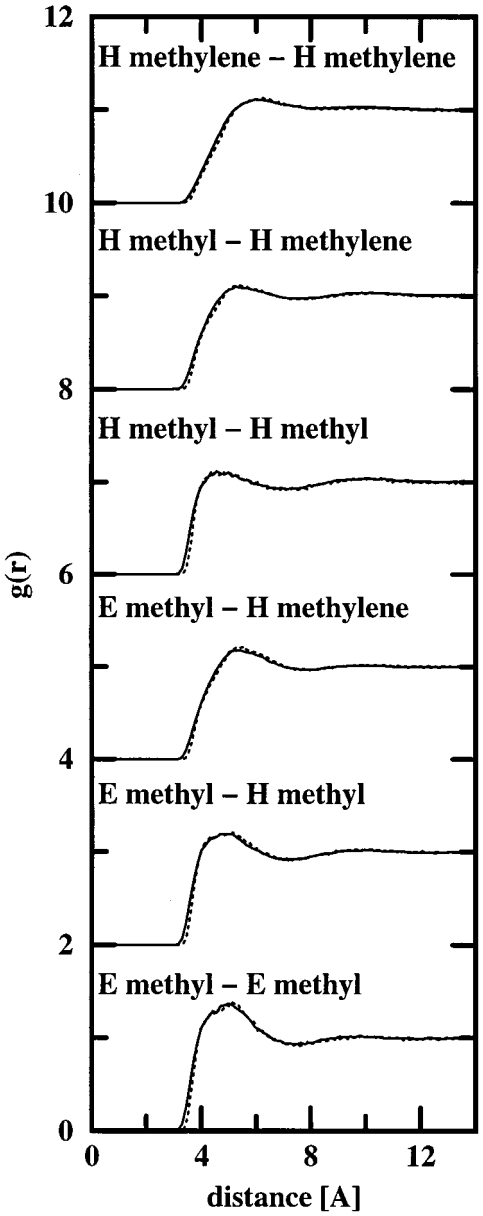

Figure 12. Carbon−carbon radial distribution functions for the liquid phase of the ethane/heptane mixture at $T = 450$ K and a pressure of 7 MPa. Radial distribution functions are shown for simulations using the TraPPE-UA (solid lines) and TraPPE-EH (dotted lines) force fields. The letters H and E denote *pesudo*-atoms or carbon atoms that belong to a given group (methyl or methylene) of *n*-heptane or ethane molecules, respectively. The results for the different group pairs are vertically displaced for clarity.

single-site to articulated-chain models, the change from a united-atom representation to an explicit-hydrogen representation has no noticeable effect on the carbon−carbon RDFs. Thus the united-atom model is able to capture all important structural features of the binary ethane/*n*-heptane mixture. The additional interaction sites on the centers of carbon−hydrogen bonds used in the TraPPE-EH model solely serve to adjust the energetics (cohesive energy, heat of vaporization, Gibbs free energy of transfer) of fluid alkane phases.[35]

5. Concluding Remarks

Configurational-bias Monte Carlo simulations in the Gibbs ensemble were performed to investigate the phase diagram and microscopic structure of (supercritical) ethane/*n*-heptane mixtures. Without introduction of any special binary mixing parameters, single-site and articulated-chain models capture the general trends of this supercritical extraction system, but the accuracy of the calculated phase diagrams is most satisfactory for the most complex molecular model, that is an explicit-hydrogen representation of the alkanes. Whereas radial distribution functions seem to show more enhanced structures for the single-site models than articulated-chain models, the corresponding number integrals are very similar for all four models. The simulations do not support a supercritical solvation mechanism that involves preferential solvation of the solute (*n*-heptane) by the supercritical solvent (ethane) or that requires nonrandom mixing of the two components. Changes in both the supercritical and liquid phases contribute significantly to the enhanced solubility of *n*-heptane in high-pressure supercritical ethane; ethane partially replaces *n*-heptane in the liquid phase ("pushing") and ethane acts as a nonspecific solvent in the supercritical phase ("pulling"). Finally, supercritical systems, which involve polar or hydrogen-bonding interactions between

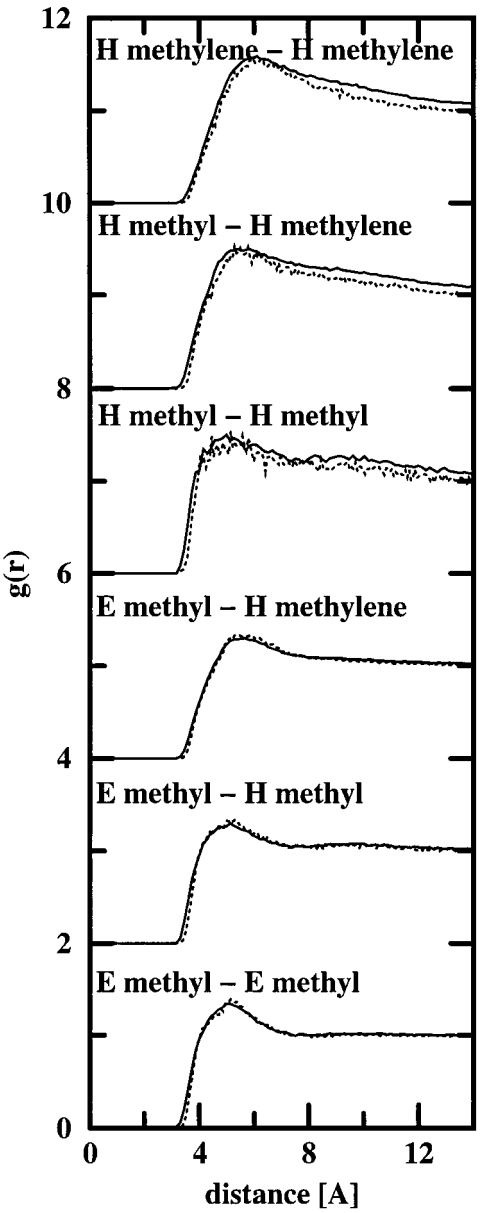

Figure 13. Carbon−carbon radial distribution functions for the supercritical phase of the ethane/heptane mixture at $T = 450$ K and a pressure of 7 MPa. Line styles and symbols as in Figure 12.

the different species, might behave differently than the simple alkane mixtures, which are governed mainly by dispersive interactions.

Acknowledgment. Financial support from the National Science Foundation (CTS-9813601), through a Camille and Henry Dreyfus New Faculty Award, a McKnight Land-Grant Professorship, and an Alfred P. Sloan Research Fellowship is gratefully acknowledged. We would like to thank the Department of Energy for a Computational Science Graduate Fellowship (M.G.M.), and the Graduate School, University of Minnesota, for the award of a Stanwood Johnston Memorial Fellowship (B.C.). Part of the computer resources were provided by the Minnesota Supercomputing Institute.

Supporting Information Available: Four tables listing the numerical values of the number integrals of the radial distribution functions at separations of 6, 8, and 10 Å. This material is available free of charge via the Internet at http://pubs.acs.org.

References and Notes

(1) Hannay, J. B.; Hogarth, J. *Proc. R. Soc. London* **1879**, *29*, 324.
(2) McHugh, M. A.; Krukonis, V. J. *Supercritical Fluid Extraction: Principles and Practice*, 2nd ed.; Butterworth: Boston, 1994.
(3) Taylor, L. T. *Supercritical Fluid Extraction*; Wiley: New York, 1996.
(4) Brunner, G. *Gas Extraction*; Steinkoff: Darmstadt, 1994.
(5) Zosel, K. French Patent 2,079, 261, 1971.
(6) Eckert, C. A.; Ziger, D. H.; Johnston, K. P.; Ellison, T. K. *Fluid Phase Equilib*. **1983**, *14*, 167.
(7) Eckert, C. A.; Ziger, D. H.; Johnston, K. P.; Kim, S. *J. Phys. Chem.* **1986**, *90*, 2738.
(8) Ekart, M. P.; Bennett, K. L.; Eckert, C. A. *ACS Symp. Ser*. **1993**, *514*, 228.
(9) Kim, S.; Johnston, K. P. *AIChE J.* **1987**, *33*, 1603.
(10) Yonker, C. R.; Frye, S. L.; Kalkwarf, D. R.; Smith, R. D. *J. Phys. Chem.* **1986**, *90*, 3022.
(11) Brennecke, J. F.; Tomasko, D. L.; Peshkin, J.; Eckert, C. A. *Ind. Eng. Chem. Res.* **1990**, *29*, 1682.
(12) Carre, O. R.; Phillips, D. J.; Brennecke, J. F. *Ind. Eng. Chem. Res.* **1994**, *33*, 1355.
(13) Zhang, J.; Lee, L. L.; Brennecke, J. F. *J. Phys. Chem*. **1995**, *99*, 9268.
(14) Pfund, D. M.; Zemanian, T. S.; Linehan, J. C.; Fluton, J. L.; Yonker, C. R. *J. Phys. Chem.* **1994**, *98*, 11846.
(15) Debenedetti, P. G.; Mohamed, R. S. *J. Chem. Phys.* **1989**, *90*, 4528.
(16) Wu, R.-S.; Lee, L. L.; Cochran, H. D. *Ind. Eng. Chem. Res.* **1990**, *29*, 977.
(17) Economou, I. G.; Donohue, M. D. *AIChE J.* **1990**, *36*, 1920.
(18) Martinez, H. L.; Ravi, R.; Tucker, S. C. *J. Chem. Phys*. **1996**, *104*, 1067.
(19) Wong, J. M.; Pearlman, R. S.; Johnston, K. P. *J. Phys. Chem*. **1985**, *89*, 2671.
(20) Johnston, K. P.; Peck, D. G.; Kim, S. *Ind. Eng. Chem. Res.* **1989**, *28*, 1115.
(21) Shing, K. S.; Chung, S. T. *J. Phys. Chem.* **1987**, *91*, 1674.
(22) Petsche, I. B.; Debenedetti, P. G. *J. Chem. Phys*. **1989**, *91*, 7075.
(23) Debenedetti, P. G. *NATO ASI Ser. E* **1994**, *273*, 439.
(24) Panagiotopoulos, A. Z. *NATO ASI Ser. E* **1994**, *273*, 411.
(25) Cummings, P. T. *NATO ASI Ser. E* **1994**, *273*, 387.
(26) Cummings, P. T.; Chialvo, A. A.; Cochran, H. D. *Chem. Eng. Sci.* **1994**, *49*, 2735.
(27) Balbuena, P. B.; Johnston, K. P.; Rossky, P. J. *J. Phys. Chem.* **1996**, *100*, 2706.
(28) Balbuena, P. B.; Johnston, K. P.; Rossky, P. J. *J. Phys. Chem.* **1996**, *100*, 2716.
(29) Gromov, D. G.; de Pablo, J. J.; Luna-Barcenas, G.; Sanchez, I. C.; Johnston, K. P. *J. Chem. Phys*. **1998**, *108*, 4647.
(30) Martin, M. G.; Siepmann, J. I. *J. Am. Chem. Soc.* **1997**, *119*, 8921.
(31) Spyriouni, T.; Economou, I. G.; Theodorou, D. N. *Phys. Rev. Lett.* **1998**, *80*, 4466.
(32) Nath, S. K.; Escobedo, F. A.; de Pablo, J. J.; Patramai, I. *Ind. Eng. Chem. Res*. **1998**, *37*, 3195.
(33) Sun, T.; Teja, A. S. *J. Phys. Chem.* **1996**, *100*, 17365.
(34) Martin, M. G.; Siepmann, J. I. *J. Phys. Chem. B* **1998**, *102*, 2569.
(35) Chen, B.; Siepmann, J. I. *J. Phys. Chem. B* **1999**, *103*, 5370.
(36) Allen, M. P.; Tildesley, D. J. *Computer Simulation of Liquids*; Oxford University Press: Oxford, 1987.
(37) Lorentz, H. A. *Ann. Phys*. **1881**, *12*, 127; Berthelot, D. *C. R. Hebd. Séances Acad. Sci. Paris* **1898**, *126*, 1703.
(38) Martin, M. G.; Siepmann, J. I. *J. Phys. Chem. B* **1999**, *103*, 4508.
(39) Van der Ploeg, P.; Berendsen, H. J. C. *J. Chem. Phys*. **1982**, *94*, 3271.
(40) Jorgensen, W. L.; Madura, J. D.; Swenson, C. J. *J. Am. Chem. Soc.* **1984**, *106*, 813.
(41) Mooij, G. C. A. M.; Frenkel, D.; Smit, B. *J. Phys. Condens. Matter* **1992**, *4*, L255.
(42) Laso, M.; de Pablo, J. J.; Suter, U. W. *J. Chem. Phys*. **1992**, *97*, 2817.
(43) Panagiotopoulos, A. Z. *Mol. Phys*. **1987**, *61*, 813.
(44) Panagiotopoulos, A. Z.; Quirke, N.; Stapleton, M.; Tildesley, D. J. *Mol. Phys.* **1988**, *63*, 527.
(45) Smit, B.; de Smedt, P.; Frenkel, D. *Mol. Phys*. **1989**, *68*, 931.
(46) Siepmann, J. I. *Mol. Phys*. **1990**, *70*, 1145.
(47) Siepmann, J. I.; Frenkel, D. *Mol. Phys*. **1992**, *75*, 59.
(48) Frenkel, D.; Mooij, G. C. A. M.; Smit, B. *J. Phys. Condens. Matter* **1992**, *4*, 3053.

(49) de Pablo, J. J.; Laso, M.; Suter, U. W. *J. Chem. Phys*. **1992**, *96*, 2395.

(50) Esselink, K.; Loyens, L. D. J. C.; Smit, B. *Phys. Rev. E* **1995**, *51*, 1560.

(51) Mackie, A. D.; Tavitian, B.; Boutin, A.; Fuchs, A. H. *Mol. Simul*. **1997**, *19*, 1.

(52) Vlugt, T. J. H.; Martin, M. G.; Smit, B.; Siepmann, J. I.; Krishna, R. *Mol. Phys.* **1998**, *94*, 727.

(53) Kay, W. B. *Ind. Eng. Chem*. **1938**, *30*, 459.

(54) Knapp, H.; Döring, R.; Oellrich, L.; Plöcker, U.; Prausnitz, J. M. *Vapor-Liquid Equilibria for Mixtures of Low Boiling Substances*; Schön and Wetzel: Frankfurt/Main, 1982.

(55) Smith, B. D.; Srivastava, R. *Thermodynamic Data for Pure Compunds: Part A Hydrocarbons and Ketones*; Elsevier: Amsterdam, 1986.